Geofísica Internacional (1998), Vol. 37, Num. 4, pp. 327-338

Error propagation in geochemical modeling of trace elements in two-component mixing

Surendra P. Verma
Centro de Investigación en Energía, UNAM, Temixco, Mor., México

Received: September 23, 1997; accepted: August 5, 1998.

RESUMEN

En este trabajo se desarrollan las ecuaciones de propagación de incertidumbres para un modelado geoquímico de elementos traza durante una mezcla de dos componentes o miembros terminales. Las ecuaciones proporcionan las incertidumbres resultantes en la concentración de un elemento o la relación de dos elementos en una mezcla de dos miembros, como función de las incertidumbres iniciales de medición. Varios ejemplos ilustran el empleo de estas ecuaciones en el modelado geoquímico. Aunque, como esperado, la concentración de un elemento o la relación de dos elementos en la mezcla se encuentra siempre entre los valores correspondientes a los dos miembros, no es el caso para las incertidumbres correspondientes de medición. La %Rsd (Desviación estándar relativa expresada en %) de la concentración de un elemento en la mezcla nunca es mayor de %Rsd del miembro con mayor incertidumbre para ese elemento, pero podría ser menor al miembro con menor incertidumbre. De la misma manera, la propagación de incertidumbres con los datos de basaltos y sedimentos de la placa de Cocos proporciona ejemplos adicionales para el empleo de estas nuevas ecuaciones y su importancia en problemas petrogenéticos.

PALABRAS CLAVE: Modelado de elementos traza, geoquímica, propagación de errores, incertidumbre de medición, mezcla, México, placa de Cocos.

ABSTRACT

This study presents error propagation equations for geochemical modeling of trace elements during mixing of two components or end-members. These equations can be used to estimate uncertainties in the concentration of an element or ratio of two elements in the mixture of two components, as a function of the initial measurement uncertainties. Several examples illustrate the use of these equations in geochemical modeling. Although as expected the element concentrations and their ratios in the mixture always lie between those of the two end-members, it is not the case with the corresponding measurement uncertainties. The %Rsd (Relative standard deviation expressed in %) of the concentration of an element in the mixture is never larger than the %Rsd of the component with larger uncertainty for that element, but can be smaller than the component with smaller uncertainty. Similarly, error propagation using actual element concentration data on basalt and sediment samples from the Cocos plate was carried out to further exemplify the use of these new equations and their importance in petrogenetic problems.

KEY WORDS: Trace element modeling, geochemistry, error propagation, measurement uncertainty, mixing, Mexico, Cocos plate.

INTRODUCTION

Mixing of two components or end-members (a term frequently used in geochemistry) is of fundamental importance in several branches of Earth Sciences, such as hydrogeology, geothermal research, geochemistry, petrology, oceanography, sedimentology, as well as in numerous laboratory and industrial procedures. Examples of such mixing processes (Faure, 1986; Albarède, 1995; Verma, 1998a) are: (i) the mingling of water of a tributary stream with that of its master stream; (ii) discharge of river water into a lake or into the oceans; (iii) mixing of two types of sediment in a depositional basin; (iv) mixing of two types of magma sources before their melting; and (v) contamination of a mantle-derived magma as a result of interactions with rocks of the Earth's crust.

The main objective is to show the effects of error propagation in the mass-conservation equations for the basic geological process of two component mixing and illustrate their use to element concentration data from subducting Cocos plate. Attention will be confined here to geochemical modeling of mixing of two-components, whose compositions are known from previous experiments and the mixture is treated as unknown.

NEW ERROR EQUATIONS FOR TWO-COMPONENT MIXING

Error propagation theory provides the rules for combining analytical errors or measurement uncertainties of two variables related to each other by a mathematical operation, such as summation, subtraction, multiplication, and division, or for a variable involved in a mathematical function, such as exponent or logarithm (Bevington, 1969; Taylor, 1982; Guedens *et al.*, 1993). Taylor (1982) uses indiscriminately the terms "Error propagation" and "Propagation of uncertainties" (see for example, the title of his book). New equa-

tions are derived from this theory by propagating measurement uncertainties of different parameters involved in geochemical modeling of mixing of two components. The resulting equations express explicitly the uncertainty of the predicted variable (concentration in the mixture) in terms of the uncertainties in the initial variables (e.g., original concentration of a trace element in source rocks, initial magmas, or a magma and an assimilant, or two different sources of waters in hydrogeological studies). These equations predict the uncertainty in the composition of the mixture of two components, prior to its possible modification from other processes that might take place after the mixing has been completed.

Equations for an element

As many other natural processes, the mixing process is controlled by mass-balance or conservation of mass. The concentration of an element *i* in the mixture C_M^i of two components (or end-members) *A* and *B* is given by:

$$C_M^i = fC_A^i + (1-f)C_B^i \qquad (1)$$

where C_A^i and C_B^i are the concentrations of element *i* (e.g., Sr or Nd or La or Pb, etc.) in the components *A* and *B* respectively, and *f* is the mass fraction of the component *A* in the mixture of *A* and *B*. The value of *f* can vary from *f*=1 for pure component *A* to *f*=0 for pure component *B*.

This equation can be rearranged to show that the concentration of an element *i* in the mixture C_M^i is a linear function of *f* as follows:

$$C_M^i = (C_A^i - C_B^i)f + C_B^i \quad . \qquad (2)$$

Let σ_A^i and σ_B^i be the associated measurement uncertainties [e.g. expressed as equivalent to one standard deviation following Taylor (1982) and Horwitz and Albert (1997)] of C_A^i and C_B^i respectively. Generally only the statistical sample standard deviations (e.g., S_A^i and S_B^i) are available and can be replaced for σ_A^i and σ_B^i respectively in the following error propagation equations. The propagated uncertainty σ_M^i on the concentration of the element *i* in the mixture C_M^i for a given value of *f* is obtained by the variance equation:

$$\sigma_M^{i^2} = f^2\sigma_A^{i^2} + (1-f)^2\sigma_B^{i^2} + 2f(1-f)\sigma_{AB}^i \qquad (3)$$

where $\sigma_A^{i^2}$ and $\sigma_B^{i^2}$ are the variances of element *i* in *A* and *B*; σ_{AB}^i is the covariance between the concentration variables C_A^i and C_B^i, which is defined as (Taylor, 1982):

$$\sigma_{AB}^i = \left\langle (C_A^i - \overline{C}_A^i)(C_B^i - \overline{C}_B^i) \right\rangle \qquad (4)$$

where $\overline{C}_A^i$ and $\overline{C}_B^i$ are the mean values of C_A^i and C_B^i respectively.

In general, the determinations of C_A^i and C_B^i are uncorrelated, and therefore σ_{AB}^i=0. The error propagation equation then simplifies to:

$$\sigma_M^{i\,2} = f^2\sigma_A^{i\,2} + (1-f)^2\sigma_B^{i\,2} \quad . \qquad (5)$$

Equation (3) for correlated or Eq. (5) for uncorrelated errors can be used to estimate the uncertainty on the predicted mixture in terms of the measurement uncertainties of individual determinations.

Equations for an element ratio

In many instances, it is advantageous to consider ratios of two elements (e.g., Sr/Nd or La/Yb or Nb/Ta or Ba/Nb, etc.). Let *i* and *j* represent two different elements. The ratio of their concentrations in the mixture is given by Eq. (7), obtained by dividing Eq. (1) by Eq. (6):

$$C_M^j = fC_A^j + (1-f)C_B^j \qquad (6)$$

$$\frac{C_M^i}{C_M^j} = \frac{fC_A^i + (1-f)C_B^i}{fC_A^j + (1-f)C_B^j} \quad . \qquad (7)$$

In general, $\frac{C_M^i}{C_M^j}$ versus *f* curve is not a straight line, but in the very special case when $C_A^j = C_B^j$, Eq. (7) reduces to:

$$\frac{C_M^i}{C_M^j} = \frac{fC_A^i + (1-f)C_B^i}{C_B^j} \quad . \qquad (8)$$

Rearranging, one has

$$\frac{C_M^i}{C_M^j} = \left(\frac{C_A^i - C_B^i}{C_B^j}\right)f + \left(\frac{C_B^i}{C_B^j}\right) \quad . \qquad (9)$$

This is a straight line. Similarly, if $C_A^i = C_B^i$, $\frac{C_M^j}{C_M^i}$ versus *f* is a straight line.

The propagated uncertainty $S_M^{i/j}$ of this ratio for the general case of correlated errors can be estimated from σ_M^i, σ_M^j and σ_M^{ij} as follows:

$$\left(\sigma_M^{i/j}\right)^2 = \left(\frac{C_M^i}{C_M^j}\right)^2\left(\frac{\sigma_M^{i\,2}}{C_M^{i\,2}} + \frac{\sigma_M^{j\,2}}{C_M^{j\,2}} - 2\frac{\sigma_M^{ij}}{C_M^i C_M^j}\right) \qquad (10)$$

where σ_M^i can be estimated from Eq. (3) for correlated errors; σ_M^j from a similar equation for element *j*; C_M^i from Eq. (1); C_M^j from Eq. (6); and σ_M^{ij}, the covariance between the concentration variables C_M^i and C_M^j, from Eq. (11):

$$\sigma_M^{ij} = \left\langle \left(C_M^i - \overline{C}_M^i\right)\left(C_M^j - \overline{C}_M^j\right) \right\rangle \quad . \tag{11}$$

As explained above, the determinations of the concentrations C_A^i and C_B^i (and similarly C_A^j and C_B^j) are independent and therefore uncorrelated. The uncorrelated nature of the variables C_A^i, C_B^i, C_A^j, and C_B^j also makes that C_M^i and C_M^j [which themselves depend on the concentration variables of the two components; see Eqs. (1) and (6)] be uncorrelated and therefore the correlated error σ_M^{ij} can be set at zero. Hence, the propagated uncertainty on the element ratio $\sigma_M^{i/j}$ can be estimated from a simplified equation (12) for variance:

$$\left(\sigma_M^{i/j}\right)^2 = \left(\frac{C_M^i}{C_M^j}\right)^2 \left(\frac{\sigma_M^{i\,2}}{C_M^{i\,2}} + \frac{\sigma_M^{j\,2}}{C_M^{j\,2}}\right) . \tag{12}$$

In this case, the parameters in Eq. (12) can be estimated as follows: σ_M^i from Eq. (5) for uncorrelated errors; σ_M^j from a similar equation for element *j*; and C_M^i and C_M^j from Eqs. (1) and (6) respectively. Therefore, Eq. (12) can be written more explicitly as:

$$\left(\sigma_M^{i/j}\right)^2 = \left(\frac{C_M^i}{C_M^j}\right)^2 \left(\frac{f^2\sigma_A^{i\,2} + (1-f)^2\sigma_B^{i\,2}}{C_M^{i\,2}} + \frac{f^2\sigma_A^{j\,2} + (1-f)^2\sigma_B^{j\,2}}{C_M^{j\,2}}\right). \tag{13}$$

Although the error propagation equations have been developed here to take into account the analytical errors or measurement uncertainties of the variables in components *A* and *B*, they could apply as well if these errors were the total uncertainties (total geological field sampling and laboratory analytical errors, including both systematic and random errors; Ramsey, 1997; Kane, 1997), reflecting total variability of the end-members and therefore of the resulting mixtures. Furthermore, these equations can also be used to model major element data during the mixing process.

RESULTS AND DISCUSSION

Illustrative examples of element concentrations

Let the concentration of a trace element *i* in component *A*, C_A^i=10 ppm and in the component *B*, C_B^i=100 ppm. Mixing of these two apparently homogeneous and measurement uncertainty-free components (C_M^i vs. *f*) is represented by a straight line [Eq. (2); Figure 1]. Obviously, this assumes that there are no uncertainties associated with the determination of these concentrations and that these components are perfectly homogeneous. Both of these assumptions are unrealistic and therefore simple models used thus far in geochemistry are fundamentally incorrect or at least statistically unreliable. Myres *et al*. (1987) noted the general problem of end-member variability and proposed a graphical approach to resolve it. In this work, a new approach involving error propagation theory has been developed and its application is illustrated below.

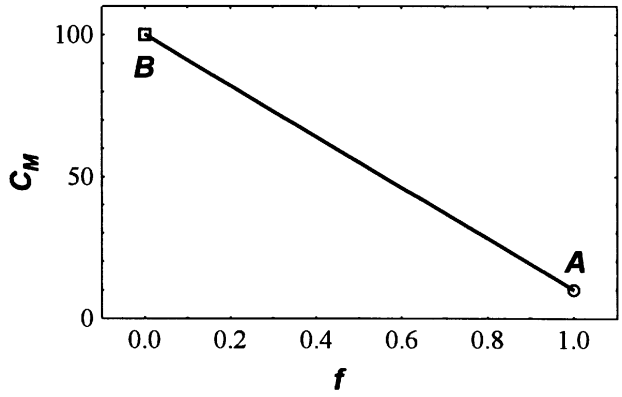

Fig. 1. Predicted concentration C_M of an element in the mixture of two components or end-members *A* and *B* as a function of *f* (*f* is the proportion of the component *A* in the mixture). C_A^i=10 ppm and C_B^i=100 ppm are assumed for this example. The component *A* is represented by a circle and the component *B* by a square in this and later diagrams. Note the mixing curve is a straight line on this diagram.

In this and later sections, two extreme cases are graphically presented. They are called: "Small uncertainties" and "Large uncertainties".

Small uncertainties: let σ_A^i=5% and σ_B^i=5% be the uncertainties (e.g. one standard deviation) on C_A^i and C_B^i respectively. Then the propagated uncertainty σ_M^i estimated from Eq. (5) is shown in Figure 2a by vertical uncertainty-bars on the mixing curve. The equal %uncertainty of 5% on unequal concentrations (extreme values of 10 ppm and 100 ppm) are reflected as uneven uncertainty-bars (Figure 2a). In this example, for low concentrations (<30 ppm), the propagated uncertainties are such that the size of the symbols generally used as data points is similar to or larger than the uncertainty-bars. However, for higher concentrations the size of these symbols is smaller than the predicted uncertainties on the mixture (Figure 2a). This uncertainty expressed as %Rsd (Relative standard deviation expressed in %) for the mixture (Figure 2b) is always lower than 5% (this being the

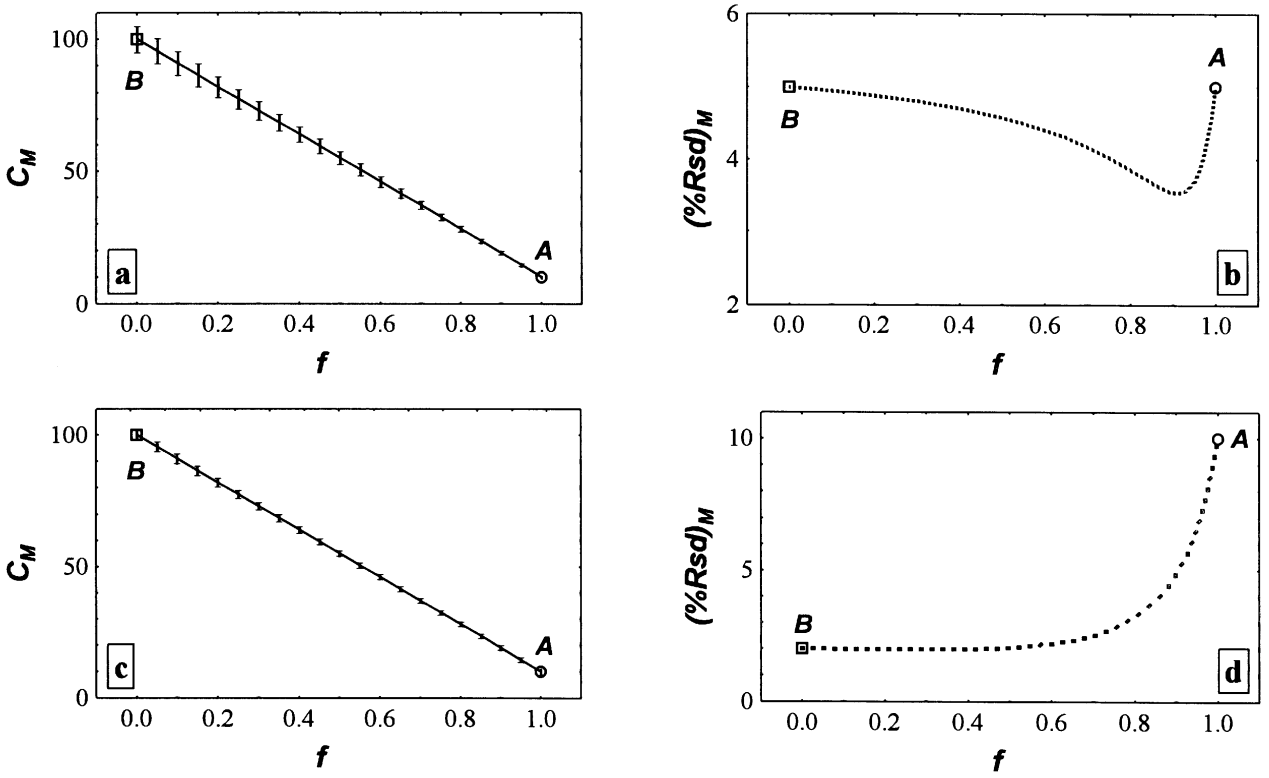

Fig. 2. Propagated uncertainty σ_M on the concentration of the mixture as a function of f for the example of Fig. 1. "Small uncertainties" examples: (a) C_M vs. f curve with σ_M vertical uncertainty-bars for σ_A=5% and σ_B=5%; (b) $(\%Rsd)_M$ vs. f curve for the same data as in Fig. 2a; (c) C_M vs. f curve with σ_M vertical uncertainty-bars for σ_A=10% and σ_B=2%; (d) $(\%Rsd)_M$ vs. f curve for the same data as in Fig. 2c.

uncertainty value assumed for the two end-members *A* and *B*) and shows a minimum value of about 3.5% for f=0.90. Note the lack of symmetry of this $(\%Rsd)_M$ vs. f curve in spite of the fact that $(\%Rsd)_A=(\%Rsd)_B$. This is due to the different concentrations of the two end-members.

Similarly, if σ_A^i=10% and σ_B^i=2%, the corresponding uncertainties on the mixture are shown in Figures 2c and 2d. The unequal %uncertainties on these concentrations (larger %uncertainty assumed, as expected, for the component having a smaller concentration) are reflected by similar uncertainty-bars in Figure 2c, as compared to the case of Figure 2a. For this example, the size of these uncertainty-bars is similar o smaller than the symbols customarily used in such graphics. The $(\%Rsd)_M$ does not show a minimum but an approximately constant uncertainty of 2% (value assumed for the component B) for f=0 to f=0.50, which then increases rapidly to the 10% value assumed for the other component (Figure 2d).

Large uncertainties: Assuming the same concentrations of elements in the two components as in the example above (Figures 1 and 2), but larger uncertainties of σ_A^i=10% and σ_B^i=30% in C_A^i and C_B^i respectively, the propagated uncertainty σ_M^i estimated from Eq. (5) is shown in Figure 3a by very large vertical uncertainty-bars on the mixing curve. The $(\%Rsd)_M$ vs. f curve (Figure 3b) shows that the relative uncertainty decreases steadily from 30% (value assumed for component *B*) at f=0 to 10% at f=1, with a small minimum of about 9.5% at f=0.99, very close to the other component.

Similarly, for σ_A^i=30% and σ_B^i=20%, the corresponding uncertainties on the mixture are shown in Figures 3c and 3d. For this example, the $(\%Rsd)_M$ shows a minimum of about 16.7% for f=0.80 (Figure 3d). In both examples, the propagated uncertainties are too large to be of much significance in most geochemical problems.

Some important points emerge from the examination of Figures 1 - 3 and the corresponding spreadsheets used for these computations (not included here for space limitations). Although, as expected, the concentration of an element in the mixture always lies between those of the two end-members, the %*Rsd* of the mixture is never larger than the %Rsd of the component with larger uncertainty, but can be smaller than the component with smaller uncertainty.

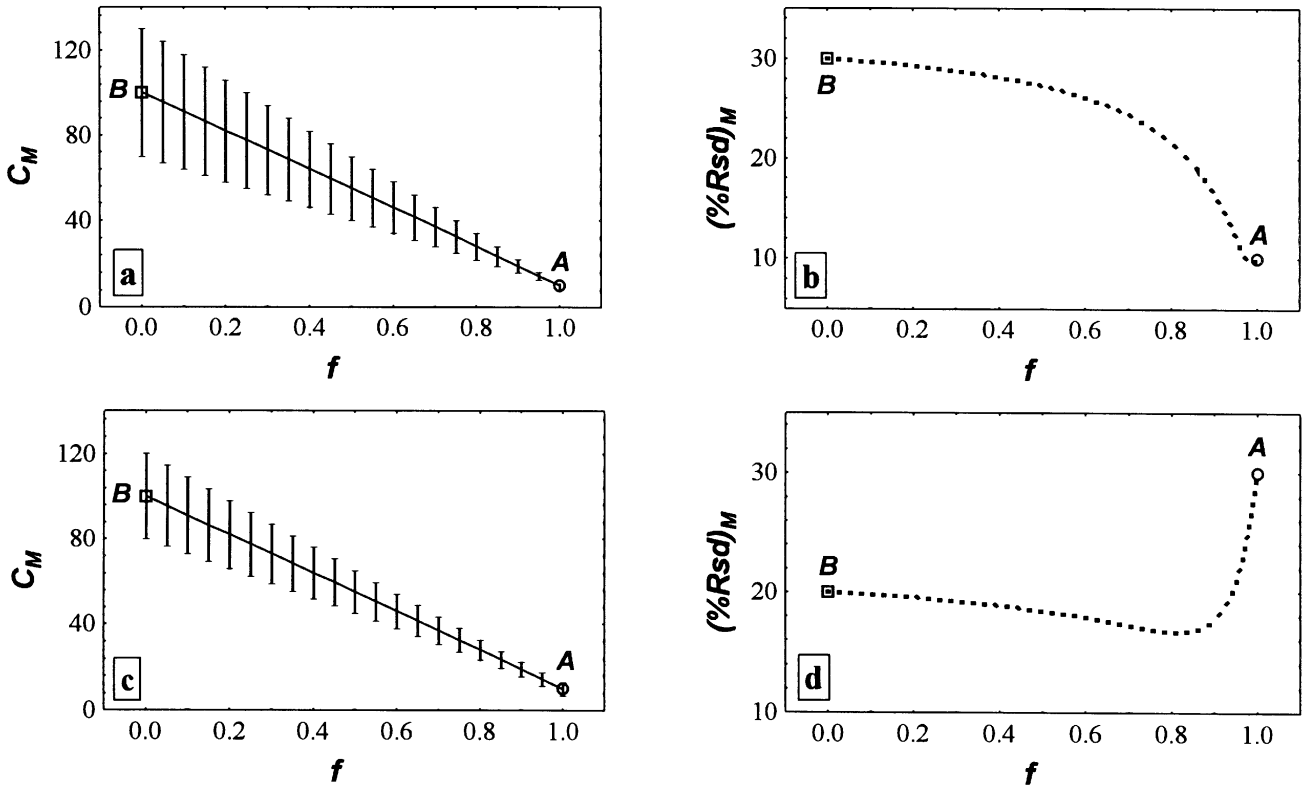

Fig. 3. Propagated uncertainty on the concentration of the mixture σ_M as a function of f for the example of Fig. 1. "Large uncertainties" examples: (a) C_M vs. f curve with σ_M vertical uncertainty-bars for σ_A=10% and σ_B=30%; (b) $(\%Rsd)_M$ vs. f curve for the same data as in Fig. 3a; (c) C_M vs. f curve with vertical uncertainty-bars for σ_A=30% and σ_B=20%; (d) $(\%Rsd)_M$ vs. f curve for the same data as in Fig. 3c.

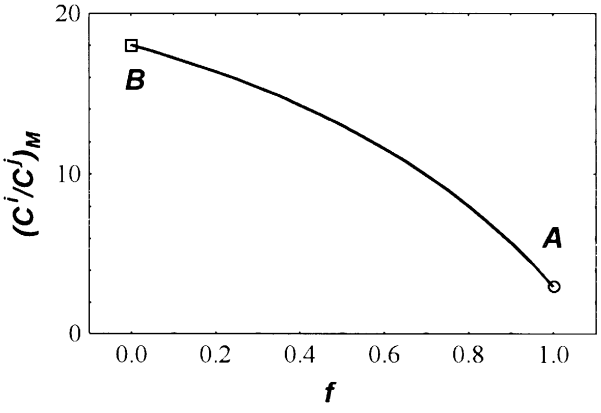

Fig. 4. Predicted ratio $(C^i/C^j)_M$ of concentrations of two elements i and j in the mixture of two components A and B as a function of f (f is the proportion of the component A in the mixture). Let C_A^i=3 ppm, C_B^i=36 ppm; C_A^j=1 ppm, and C_B^j=2 ppm. Therefore; $\frac{C_A^i}{C_A^j}$=3 and $\frac{C_B^i}{C_B^j}$=12 are assumed for this example. Note the mixing curve is *not* a straight line.

Illustrative examples of ratio of two element concentrations

A general mixing curve is presented in Figure 4. For this example, the concentration of a trace element i in components A and B are taken as: C_A^i=3 ppm and C_B^i=36 ppm. Similarly, for element j, the respective concentrations are: C_A^j=1 ppm and C_B^j=2 ppm. The mixing of these two apparently "homogeneous and uncertainty-free" components $[C^i/C^j)_M$ vs. f curve] is in general not represented by a straight line [Eq. (7); Figure 4]. As before, two extreme cases are graphically presented: Small uncertainties (Figures 5a and 5b) and Large uncertainties (Figures 5c and 5d).

Small uncertainties: This case is for σ_A^i=10%, σ_B^i=5%, σ_A^j=2%, σ_B^j=2%. The propagated uncertainty $\sigma_M^{i/j}$ estimated from Eq. (13) is shown in Figure 5a by vertical uncertainty-bars on the mixing curve. The results for the small uncertainties assumed here are shown in Figure 5b, as total propagated uncertainties on the concentration ratio expressed as $(\%Rsd)_M$. The uncertainties vary from about 5.4% for pure component B (f=0) to 10.2% for pure component A (f=1), passing through a minimum value of about 4.7% at f=0.75.

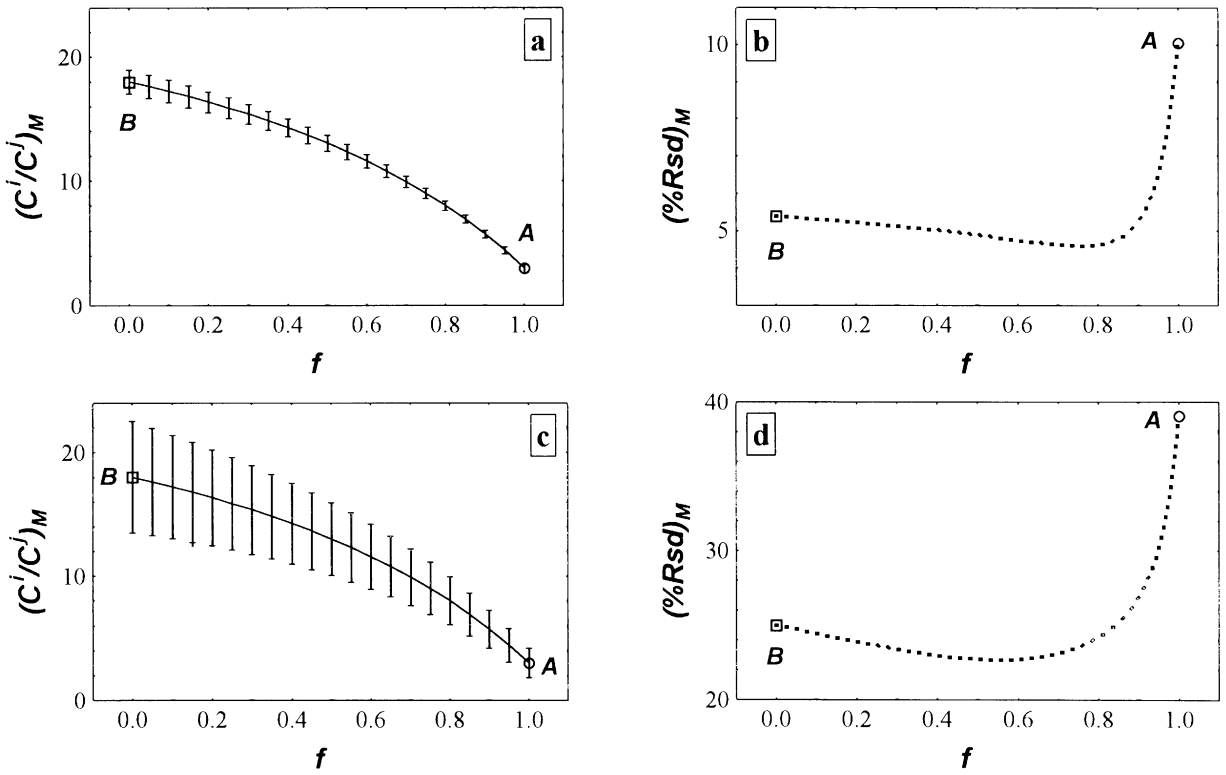

Fig. 5. Propagated uncertainty $\sigma_M^{i/j}$ (shown as vertical uncertainty-bars) on the ratio of the concentrations of two elements in the mixture $(C^i/C^j)_M$ as a function of f for the example of Figure 4. "Small uncertainties" example: (a) propagated uncertainty shown by vertical uncertainty-bars for σ_A^i=10%, σ_B^i=5%; σ_A^j=1%, and σ_B^j=2%; (b) $(\%Rsd)_M$ vs. f curve for the same data as in Fig. 5a. "Large uncertainties" example: (c) Vertical uncertainty-bars for σ_A^i=30%, σ_B^i=20%; σ_A^j=25%, and σ_B^j=15%; (d) $(\%Rsd)_M$ vs. f curve for the same data as in Fig. 5c.

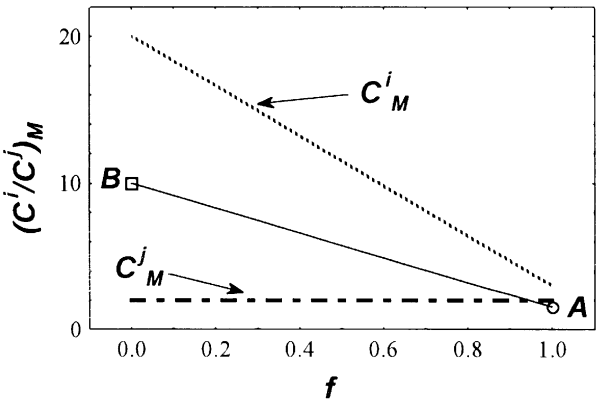

Fig. 6. Predicted concentration ratio $(C^i/C^j)_M$ of two elements i and j in the mixture of two components A and B as a function of f for the very special case when the mixing curve is a straight line. C_A^i=3 ppm, C_B^i=20 ppm; C_A^j=2 ppm, and C_B^j=2 ppm. Therefore, $\frac{C_A^j}{C_B^j}$=1 (the condition required for the mixing curve to be a straight line) and $\frac{C_B^i}{C_B^j}$=10 are assumed for this example.

Large uncertainties: Assuming the same concentrations (Figure 4) but larger uncertainties of σ_A^i=30% and σ_B^i=20%, σ_A^j=25%, σ_B^j=15%, the results are shown in Figures 5c and 5d. As expected, the propagated uncertainty (Figure 5c) is represented by very large vertical uncertainty-bars on the mixing curve. The $(\%Rsd)_M$ vs. f curve (Figure 5d) shows that the relative uncertainty decreases slightly from 25.0% at f=0 to 22.7% at f=0.55 and then increases rapidly to about 39.1% at f=1.

A straight line can result for a mixing curve under very special circumstances when the concentration of an element in both components is identical (Figure 6). The mixing curve AB corresponds to: C_A^i=3 ppm, C_B^i=20 ppm, C_A^j=2 ppm, and C_B^j=2 ppm. Besides the $[C^i/C^j)_M$ vs. $f]$ straight line AB, The individual mixing lines C_M^i and C_M^j for the concentrations of these two elements are also shown in Figure 6.

Small uncertainties: This case is for σ_A^i=10%, σ_B^i=5%, σ_A^j=1%, σ_B^j=2%. The propagated uncertainty $\sigma_M^{i/j}$ is shown in Figure 7a by vertical uncertainty-bars on the mixing curve. The $(\%Rsd)_M$ varies from about 5.4% for pure component B

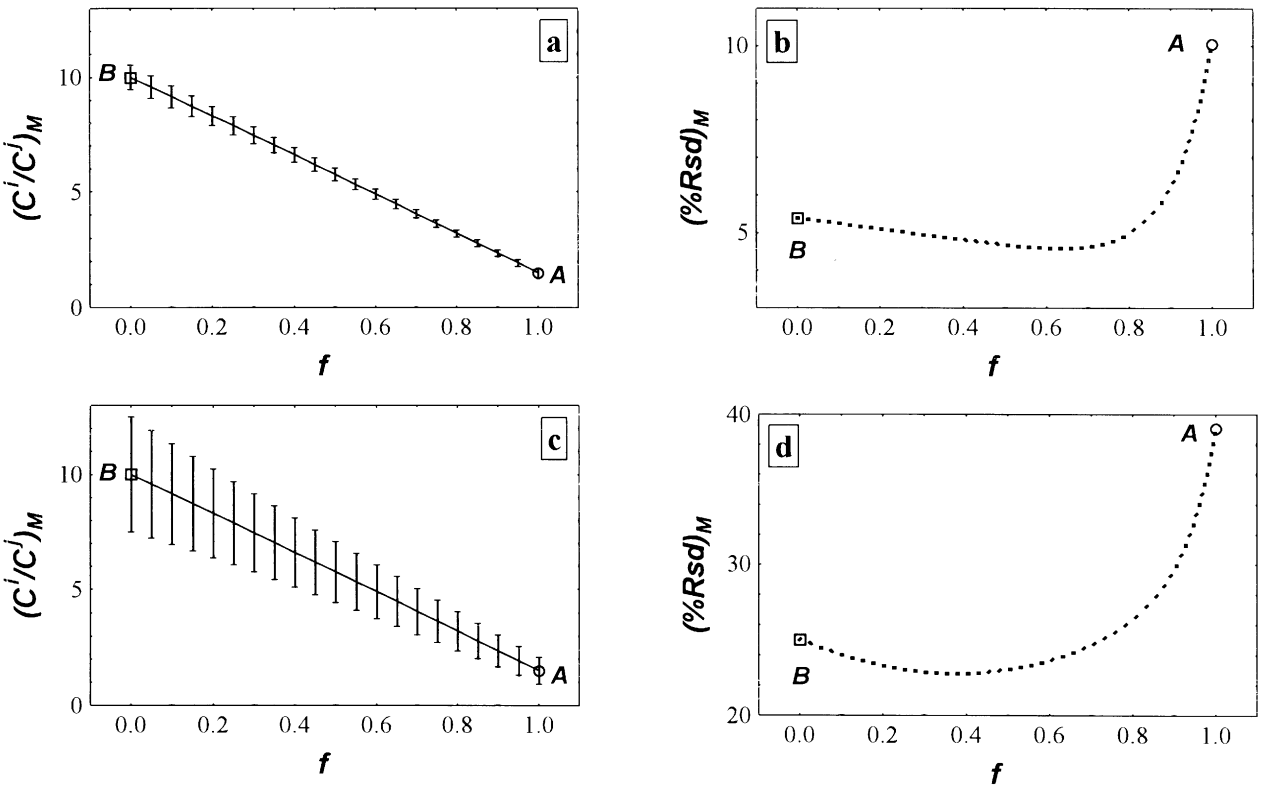

Fig. 7. Propagated uncertainty $\sigma_M^{i/j}$ (shown as vertical uncertainty-bars) on the ratio of the concentrations of two elements in the mixture $(C^i/C^j)_M$ as a function of *f* for the example of Fig. 6. "Small uncertainties" example: (a) Vertical uncertainty-bars for σ_A^i=10%, σ_B^i=5%; σ_A^j=1%, and σ_B^j=2%; (b) $(\%Rsd)_M$ vs. *f* curve for the same data as in Fig. 7a. "Large uncertainties" example: (c) vertical uncertainty-bars for σ_A^i=30%, σ_B^i=20%; σ_A^j=25%, and σ_B^j=15%; (d) $(\%Rsd)_M$ vs. *f* curve for the same data as in Fig. 7c.

(*f*=0) to 10.0% for pure component *A* (*f*=1), passing through a minimum value of about 4.6% at *f*=0.65.

Large uncertainties: Assuming the same concentrations (Figure 6) but larger uncertainties of σ_A^i=30% and σ_B^i=20%, σ_A^j=25%, σ_B^j=15%, the results are shown in Figures 7c and 7d. The $(\%Rsd)_M$ vs. *f* curve (Figure 7d) shows that the relative uncertainty decreases slightly from 25.0% at *f*=0 to 22.8% at *f*=0.40 and then increases rapidly to about 39.1% at *f*=1.

The examples presented above illustrate the effect of uncertainties and show the need of high quality data for them to be useful in geochemical modeling. It is clear from numerous diagrams that with "large uncertainties", the uncertainty-bars on the mixing curve are too large to be of much use in such modeling. This point is not trivial, because even today many laboratories, not only in Mexico but in other countries as well, keep on generating data without a clear mention and test of their quality. Such data are likely to be of little use in constraining geochemical models.

Application to concentration data from the Cocos plate

Further examples using actual data for basalt and sediment samples from the Cocos plate (Verma, 1998b) are presented to further exemplify the use of these error propagation equations. The samples come from IPOD-DSDP Site 487 drilled at the Cocos plate, in the Pacific ocean, about 11 km seaward from the Middle America Trench, off Acapulco, Mexico. The upper about 105 m thick layer was hemipelagic gray mud (cores 1-12) and overlies about 65 m thick pelagic brown clay (cores 13-19). Below the sediment cover, during drilling of about 20 m of basement rocks two meters of basalt fragments were recovered at this Site. These altered Mid-Ocean Ridge basalt (MORB) samples are mainly fine-grained plagioclase-olivine phyric basalt, with minor amount of aphyric basalt.

Two composite samples were analyzed by Verma (1998b) by X-ray fluorescence spectrometry (XRF). The sediment-composite was a physical mixture of six sediment samples from this Site (cores 6-19) and can be taken as representative of the sedimentary section of the subducting Cocos plate. The MORB-composite was also a physical mixture of six basalt samples from cores 20 and 21. The results are summarized in Table 1. Although the analytical data are of generally high quality, Ba and Nb concentrations in

Table 1

Trace element data (with analytical errors) in MORB and sediment samples from DSDP Site 487 located at the Cocos plate, Mexico (summarized from Verma, 1998b).

Element	Sediment-composite			MORB-composite		
	C_A	$\pm s_A$	$(\%Rsd)_A$	C_B	$\pm s_B$	$(\%Rsd)_B$
Ba	1639	± 4	0.2	7	± 1	14
Nb	8.6	± 0.1	1.2	1.5	± 0.7	47
Zr	112	± 2	1.8	36	± 1	2.8
Y	43.5	± 0.6	1.4	23.0	± 0.4	1.7
Sr	204	± 2	1.0	65	± 1	1.5
Rb	92	± 2	2.2	3.0	± 0.2	6.7
Zn	250	± 1	0.4	80	± 1	1.2
Cu	240	± 1	0.4	96	± 1	1.0
Ni	145	± 1	0.7	114	± 1	0.9
Co	19.5	± 0.7	3.6	42	± 1	2.4
Cr	66	± 1	1.5	420	± 2	1.2
V	173	± 1	0.6	247	± 2	0.8

S_A and S_B are one standard deviation values of the concentration data C_A and C_B respectively; $(\%Rsd)_A$ and $(\%Rsd)_B$ are the relative standard deviations in % of the components *A* and *B* respectively; the sediment-composite analyzed was a physical mixture of equal weights of six sediment samples; similarly, the MORB-composite was also a physical mixture of equal weights of six altered basalt samples from Site 487.

MORB-composite are characterized by large uncertainties, which is due to the analytical difficulty of XRF at such low concentrations.

Individual samples were also analyzed by Verma (1998b) for major elements by XRF and rare-earth elements by high-performance liquid chromatography. A summary of these and other results from the literature is presented in Table 2. The two sets of analytical results with corresponding uncertainties (analytical random errors in Table 1 and total uncertainties of geological field sampling and analytical errors in Table 2) are used to demonstrate the use of the equations derived in this work. The propagated uncertainties on the concentrations here reflect the combined effect of sample heterogeneity and analytical uncertainties. The predicted mixtures of MORB and brown clay sediment will reflect the role of heterogeneous end-members in this process.

The results of the concentration data in three mixtures are given in Tables 3 and 4. For the data of Table 3, mixtures of MORB-composite and sediment-composite were considered: M1SC (99% MORB with 1% sediment); M5SC (95% and 5%) and M20SC (80% and 20%). Thus they contain respectively 1%, 5% and 20% sediment component (designated as component *B* in earlier Figures). These three mixtures were chosen because, as demonstrated through radiogenic isotope modeling by Verma (1998b), the participation of the sediment component can not exceed about 20%.

The large uncertainties associated with the Nb data in MORB (Table 1) and reflected in the predicted mixtures (Table 3) are to be noted. This makes the present set of Nb data much less useful for geochemical modeling, as the differences in predicted Nb concentrations of the three mixtures are not significant in the light of these large propagated uncertainties. This example clearly demonstrates the usefulness of error propagation in conjunction with conventional geochemical modeling of magmatic processes.

The other trace element concentration data for the mixtures (Table 3) seem to be of high quality. However, only certain elements, such as Ba, Sr, and Rb, show large contrast (as compared to the analytical uncertainties) in order to be useful for constraining the sedimentary component.

Table 2

Major and trace element data (with total sampling and analytical errors) in MORB and sediment samples from DSDP Site 487 located at the Cocos plate, Mexico (summarized from Verma, 1998b).

Element	Brown clay sediment				MORB			
	n	C_A	s_A	$(\%Rsd)_A$	n	C_B	s_B	$(\%Rsd)_B$
SiO_2	4	38.7	1.7	4.4	17	48.2	0.7	1.5
TiO_2	4	0.34	0.09	26	17	0.85	0.03	3.5
Al_2O_3	4	9.66	0.46	4.8	17	16.9	0.5	3.0
$Fe_2O_3^t$	4	12.6	3.4	27	17	9.82	0.44	4.5
MnO	4	2.9	1.2	41	17	0.17	0.10	59
MgO	4	2.34	0.66	28	17	7.96	0.83	10
CaO	4	1.59	0.60	38	17	13.29	0.40	3.0
Na_2O	4	3.92	0.79	20	17	1.98	0.44	22
K_2O	4	1.75	0.36	21	17	0.14	0.04	29
P_2O_5	4	0.40	0.09	22	17	0.08	0.04	50
LOI	4	25.1	4.4	0.6	17	1.45	0.61	42
La	3	47	10	21	5	2.23	0.65	29
Ce	3	36	10	28	5	4.8	1.1	23
Pr	3	10.5	2.5	24	5	0.77	0.14	18
Nd	3	40	10	25	5	4.17	0.56	13
Sm	3	8.9	2.2	25	5	1.47	0.13	8.8
Eu	3	2.3	0.6	26	5	0.59	0.02	3.4
Gd	3	10.2	2.3	23	5	2.29	0.14	3.1
Tb	3	1.56	0.37	24	5	0.46	0.02	4.3
Ho	3	2.19	0.40	18	5	0.67	0.07	10
Er	3	6.2	1.2	19	5	2.04	0.29	14
Tm	3	0.90	0.10	11	5	0.29	0.05	17
Yb	3	6.3	1.0	16	5	1.98	0.30	15
Lu	3	0.91	0.08	8.8	5	0.32	0.06	19
Nb	-	-	-	-	3	0.4	0.2	50
Sr	24	362	121	33	3	55	1	1.8
Zn	24	287	64	22	3	61	1	1.6
Ni	24	260	82	32	3	129	10	7.8
Co	24	51	14	27	3	45	1	2.2
Cr	24	93	33	35	3	453	7	1.5
V	24	328	114	35	3	243	11	4.5

n= number of individual sample determinations; for more explanation, see Table 1.

For the results of modeling reported in Table 4, the components were represented by average compositions of several individual samples included in Table 2. Some of these elements, such as SiO_2, TiO_2, Co, V, and heavy REE from Tb to Lu, are characterized by small uncertainty but do not seem to vary significantly in the three mixtures (Table 4). On the other hand, the elements, such as Sr, Zn, and light REE La to Nd, show large variations in these three mixtures (above the total propagated uncertainties) and therefore should prove more useful in constraining the mixing process.

Table 3

Some predicted mixture of MORB and sediment samples compositions (with their errors estimated from the error propagation theory) using initial end-member data from Table 1.

Elem.	M1SC			M5SC			M10SC		
	C_M	$\pm s_M$	$(\%Rsd)_M$	C_M	$\pm s_M$	$(\%Rsd)_M$	C_M	$\pm s_M$	$(\%Rsd)_M$
Ba	23.3	± 1.0	4.2	88.6	± 1.0	1.1	333.4	± 1.1	0.3
Nb	1.6	± 0.7	44	1.9	± 0.7	36	2.9	± 0.6	19
Zr	36.8	± 1.0	2.7	39.8	± 1.0	2.4	51.2	± 0.9	1.7
Y	23.20	± 0.40	1.7	24.02	± 0.38	1.6	27.10	± 0.34	1.3
Sr	66.4	± 1.0	1.5	72.0	± 1.0	1.3	92.8	± 0.9	1.0
Rb	3.89	± 0.20	5.1	7.45	± 0.22	2.9	20.80	± 0.43	2.1
Zn	81.9	± 1.0	1.2	88.5	± 1.0	1.1	114.0	± 0.8	0.7
Cu	97.4	± 1.0	1.0	103.2	± 1.0	0.9	124.8	± 0.8	0.7
Ni	114.3	± 1.0	0.9	115.6	± 1.0	0.8	120.2	± 0.8	0.7
Co	41.8	± 1.0	2.4	40.9	± 1.0	2.3	37.5	± 0.8	2.2
Cr	416	± 5	1.2	402	± 5	1.2	349	± 4	1.1
V	246.3	± 2.0	0.8	243.3	± 1.9	0.8	232.2	± 1.6	0.7

M1SC = Mixture of 99% of MORB-composite with 1% of sediment-composite;
M5SC = Mixture of 95% of MORB-composite with 5% of sediment-composite;
M20SC = Mixture of 80% of MORB-composite with 20% of sediment-composite.

Application to element ratios from the Cocos plate

Some examples of ratios of these elements are reported in Table 5. The first set of propagated uncertainties reflects the effect of analytical errors, whereas the second set shows the consequences of total uncertainties (geological field sampling and analytical errors). The TiO_2/V ratio included in both sets permits a quick comparison of these data. The results of the Ba/Nb ratio show the propagation of large uncertainty of Nb in the MORB-composite. However, this ratio shows a very large contrast between the two end-members used in the mixing calculations and therefore seems to be useful for constraining the sediment component in spite of the large propagated uncertainties (Table 5). Nevertheless, when one looks carefully at the results of error propagation, the need for high quality experimental data becomes obvious if they are to be used for geochemical modeling. The usefulness of the error propagation theory is also demonstrated from the Mexican geochemical data. The results of the element concentrations and their ratios in the mixtures of basalt and sediment samples from the Cocos plate, along with the propagated uncertainties, will be used in models of partial melting and fractional crystallization to better constrain the magma genesis in the Mexican Volcanic Belt. They will constitute examples of application of these processes in future papers of this series.

CONCLUSIONS

Error propagation theory is successfully applied to trace element modeling in order to predict the effects of analytical uncertainties in trace element determination. Two probable (extreme) cases identified by "*Small uncertainties*" and "*Large uncertainties*" are presented to illustrate the use of the newly derived error propagation equations for two-component mixing. The results are presented graphically to show the effect of error propagation in geochemical modeling. Actual example of geochemical data from the Cocos plate is presented to demonstrate the usefulness of this approach in geochemical modeling.

ACKNOWLEDGEMENTS

This work was partly supported by CONACyT project 0196P-T and DGAPA project IN-100596. B. Stewart is

Table 4

Some predicted mixture of MORB and sediment samples compositions (with their errors estimated from the error propagation theory) using initial end-member data from Table 2.

Elem.	M1S			M5S			M10S		
	C_M	$\pm s_M$	$(\%Rsd)_M$	C_M	$\pm s_M$	$(\%Rsd)_M$	C_M	$\pm s_M$	$(\%Rsd)_M$
SiO_2	48.1	± 0.7	1.4	47.7	± 0.7	1.4	46.3	± 0.7	1.4
TiO_2	0.84	± 0.03	3.5	0.82	± 0.03	3.5	0.75	± 0.03	4.0
Al_2O_3	16.8	± 0.5	2.9	16.5	± 0.5	2.9	15.45	± 0.41	2.7
$Fe_2O_3^t$	9.85	± 0.44	4.4	10.0	± 0.5	4.5	10.4	± 0.8	7.4
MnO	0.20	± 0.10	51	0.31	± 0.11	37	0.72	± 0.25	35
MgO	7.9	± 0.8	10	7.7	± 0.8	10	6.8	± 0.7	9.9
CaO	13.17	± 0.40	3.0	12.70	± 0.38	3.0	10.95	± 0.34	3.1
Na_2O	2.00	± 0.44	22	2.08	± 0.42	20	2.37	± 0.39	16
K_2O	0.16	± 0.04	25	0.22	± 0.04	19	0.46	± 0.08	17
P_2O_5	0.08	± 0.04	48	0.10	± 0.04	40	0.14	± 0.04	25
LOI	1.7	± 0.6	36	2.6	± 0.6	24	6.2	± 1.0	16
La	2.7	± 0.7	24	4.5	± 0.8	18	11.2	± 2.1	18
Ce	5.1	± 1.1	21	6.4	± 1.2	18	11.0	± 2.2	20
Pr	0.87	± 0.14	16	1.26	± 0.18	15	2.7	± 0.5	19
Nd	4.5	± 0.6	12	6.0	± 0.7	12	11.3	± 2.1	18
Sm	1.54	± 0.13	8.5	1.84	± 0.16	9.0	3.0	± 0.5	15
Eu	0.61	± 0.02	3.4	0.68	± 0.04	5.3	0.93	± 0.12	13
Gd	2.37	± 0.14	5.9	2.69	± 0.18	6.5	3.9	± 0.5	12
Tb	0.47	± 0.02	4.3	0.52	± 0.03	5.1	0.68	± 0.08	11
Ho	0.68	± 0.07	10	0.75	± 0.07	9.3	0.97	± 0.10	10
Er	2.08	± 0.29	14	2.25	± 0.28	13	2.87	± 0.33	12
Tm	0.30	± 0.05	17	0.32	± 0.05	15	0.41	± 0.04	11
Yb	2.02	± 0.30	15	2.20	± 0.29	13	2.84	± 0.31	10
Lu	0.33	± 0.06	18	0.35	± 0.06	16	0.44	± 0.05	12
Sr	58.1	± 1.6	2.7	70	± 6	8.7	116	±24	21
Zn	63.3	± 1.2	1.9	72.3	± 3.3	4.6	106	±13	12
Ni	130	±10	7.6	136	±10	7.6	155	±18	12
Co	45.1	± 1.0	2.2	45.3	± 1.2	2.6	46.2	± 2.9	6.3
Cr	449	± 7	1.5	435	± 7	1.6	381	± 9	2.3
V	244	±11	4.5	247	±12	4.8	260	±24	9.4

The mixtures M1S, M5S, and M20S are similar to those of Table 3, with the difference that average values for multiple sampels (MORB and brown clay sediment) were used instead of composite samples.

thanked for suggestions to include examples of a case study in order to demonstrate better the use of such error propagation equations. I am also grateful to C. Lomnitz and an anonymous reviewer for constructive comments on an earlier version of this paper.

Table 5

Some predicted element ratios (with their errors estimated from the error propagation theory) in mixtures of MORB and sediment samples from the Cocos plate, Mexico.

Ratio	MORB			Sediment			M1SC or M1S			M5SC or M5S			M20SC or M20S		
	$C_A^{i/j}$	s_A	$(\%Rsd)_A$	C_B	s_B	$(\%Rsd)_B$	C_M	s_M	$(\%Rsd)_M$	C_M	s_M	$(\%Rsd)_M$	C_M	s_M	$(\%Rsd)_M$
Initial errors: Analytical errors (initial trace element data from Tables 1 and 3)															
Ba/Nb	4.7	2.3	49	191	2	1.2	15	7	44	48	17	36	114	22	19
Sr/Rb	21.7	1.5	6.8	68	5	6.7	22.1	1.5	6.8	24.0	1.6	6.8	30.9	2.1	6.7
$1000TiO_2/V$	3.44	0.12	3.6	2.0	0.5	26	3.43	0.12	3.6	3.39	0.12	3.6	3.22	0.13	4.1
Initial errors: Sampling and analytical errors (major and trace data from Tables 2 and 4)															
La/Yb	1.13	0.37	33	7.5	2.0	27	1.32	0.38	28	2.0	0.5	22	3.9	0.8	21
La/Sm	1.5	0.5	30	5.3	1.7	33	1.73	0.45	26	2.4	0.5	20	3.8	0.9	24
$1000TiO_2/V$	3.50	0.20	5.7	1.0	0.5	44	3.46	0.20	5.7	3.33	0.20	6.0	2.88	0.29	10

The mixtures M1SC, M5SC, and M20SC are same as in Table 3; M1S, M5S, and M20S are same as in Table 4.

BIBLIOGRAPHY

ALBARÈDE, F., 1995. Introduction to Geochemical Modeling, Cambridge University Press, Cambridge, 543 p.

BEVINGTON, P.R., 1969. Data Reduction and Error Analysis for the Physical Sciences, McGraw Hill, New York, 336 p.

FAURE, G., 1986. Principles of Isotope Geology, second edition, John Wiley, New York, 589 p.

GUEDENS, W.J., J. YPERMAN, J. MULLENS, L.C. VAN POUCKE and E.J. PAUWELS, 1993. Statistical analysis of errors: a practical approach for an undergraduate Chemistry lab. Part 1. The concepts. *J. Chem. Educ. 70*, 776-779.

HORWITZ, W. and R. ALBERT, 1997. The concept of uncertainty as applied to chemical measurements. *Analyst, 122*, 615-617.

KANE, J.S., 1997. Analytical bias: the neglected component of measurement uncertainty. *Analyst, 122*, 1283-1288.

MYERS, J.D., C.L. ANGEVINE, and C.D. FROST, 1987. Mass balance calculations with end member compositional variability: applications to petrologic problems. *Earth Planet. Sci. Lett. 81*, 212-220.

RAMSEY, M.H., 1997. Measurement uncertainty arising from sampling: implications for the objectives of geoanalysis. *Analyst, 122*, 1255-1260.

TAYLOR, J.R., 1982. An Introduction to Error Analysis. The Study of Uncertainties in Physical Measurements. University Science Books, New York, 269 p.

VERMA, S.P., 1998a. Error propagation in equations for geochemical modeling of radiogenic isotopes in two-component mixing. *Proc. Ind. Acad. Sci. (Earth Planet. Sci.)*, in press.

VERMA, S.P., 1998b. Geochemistry of subducting Cocos plate and the origin of subduction-unrelated mafic volcanism at the volcanic front of central Mexican Volcanic Belt. *Geol. Soc. Am. Spec. Paper, 334*, on Cenozoic Volcanism and Tectonics of Mexico, in press.

Surendra P. Verma
Centro de Investigación en Energía, UNAM, Priv. Xochicalco S/N, Col. Centro, A. P. 34, Temixco, Mor. 62580, Mexico.
Email: spv@mazatl.cie.unam.mx